Nonlinear optical phase conjugation

Martial Ducloy

Laboratoire de Physique des Lasers, Université Paris-Nord, France

Summary: This article summarizes the nonlinear optical methods allowing one to perform optical phase conjugation, *i.e.* spatial-phase reversal of an incoming electromagnetic wave. Special attention is given to the most powerful technique – to date – which is based on degenerate four-wave mixing (DFWM). One discusses the physical processes (one-photon and two-photon resonances) responsible for DFWM. The generation of light-induced Bragg gratings, and the analogy with real-time holography are emphasized, with a brief review of the applications in adaptive optics and imaging (wavefront rectification, etc.). Also described are the spectroscopic applications of DFWM (transient gratings, Doppler-free emission in gases, high-frequency heterodyne spectroscopy), the polarization properties of phase-conjugate mirrors, and the operation of phase-conjugate resonators.

1 Introduction

The generation of an optical wave which is "phase-conjugate" or "time-reversed" of an incident wave by means of non-linear optical processes has been proposed in the early 70's by several research teams [1–3]. These methods and their applications, now described under the general appelation "phase-conjugate optics", have undergone a tremendous development in the last five years and span as various research fields as adaptive optics, real-time holography, interferometry, high resolution spectroscopy, laser-induced instabilities, wave propagation in the atmosphere, laser fusion, etc. In this article, we first present the principle of phase conjugate (PC) mirrors, and its practical consequences. After a brief discussion of the nonlinear processes which have been used for phase conjugation, the rest of this article will be devoted to the most powerful technique, namely degenerate four-wave mixing (DFWM) [4]. We will present the physical processes responsible for degenerate four-wave mixing, its analogy with real-time holography and its use for wavefront rectification, the spectroscopic applications of DFWM, the polarization characteristics of PC mirrors based on DFWM, and finally the properties of phase-conjugate resonators [5].

2 The phase-conjugate (PC) mirror

An ideal "phase-conjugator" transforms an incident electromagnetic (e.m.) field into an e.m. field exhibiting the same time-dependence but with a reversed spatial

phase. For instance, from an incident monochromatic wave,

$$\vec{E}_0(\vec{r}, t) = \mathrm{Re}\,[\vec{A}_0(\vec{r})\, e^{i\omega t}] \tag{1}$$

the ideal phase-conjugator generates a wave having the same frequency, but a conjugate spatial dependence:

$$\vec{E}_r(\vec{r}, t) = \mathrm{Re}\,[\vec{A}_0^*(r)\, e^{i\omega t}] \tag{2}$$

Then it acts like a special *mirror*, since a plane wave (wavevector $\vec{k}_0$, phase φ_0 and polarisation $\vec{e}_0$) is reflected with opposite wavevector $\vec{k}_r = -\vec{k}_0$, opposite phase $-\varphi_0$ and complex conjugate polarisation, $\vec{e}_0^*$:

$$\vec{A}_r = \vec{A}_0^* = \vec{e}_0^*\, \epsilon_0\, e^{i(\vec{k}_0 \cdot \vec{r} - \varphi_0)} \tag{3}$$

The PC mirror reflects a wavefront identical to the incident one, since each wavevector $\vec{k}_0$ is transformed into its opposite. For instance, a diverging wave striking a PC mirror is converted to a *converging* one, contrary to what happens with an ordinary mirror (Fig. 1). This property is easily understood if one realizes that $\vec{E}_r$ can be considered as the time-reversed of $\vec{E}_0$, at the position of the PC mirror:

$$\vec{E}_r(\vec{r}, t) = \vec{E}_0(\vec{r}, -t) \tag{4}$$

The propagation laws of the e.m. field imply that it is verified everywhere, and thus oblige the conjugate field to retrace back the path of the incident field. In particular, any deformation experienced by the incident wavefront through an aberrating medium (such as a non-uniform glass plate, a turbulent atmosphere or an irregular optical fiber etc.) will be transmitted (with phase reversal) to the reflected beam by the PC mirror, and thus rectified after a second transit in the aberrating medium (Fig. 2). This opens the way to *real-time wavefront rectification*, and the restoration of distorted images to their original state. This property should have applica-

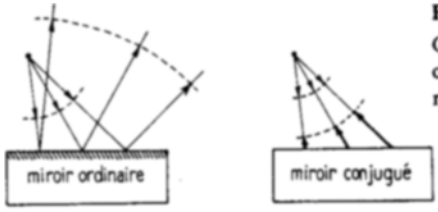


Fig. 1
Comparison between the reflexions of a diverging wavefront on an ordinary mirror and a conjugate mirror.

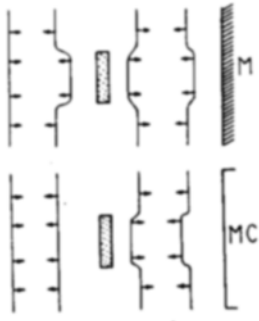


Fig. 2
The phase delay imposed to an incident plane wavefront by a glass plate is transformed by the "phase-conjugate mirror" (MC) into a phase advance which is thus exactly canceled in the return way. On the opposite, for an ordinary mirror (M), the two phase delays add in the e.m. wave round trip.

tions each time that an optical beam is distorted during its propagation: propagation in the atmosphere, information and image transmission in optical fibers, automatic pointing and focussing on a target, laser fusion, photolithography, etc. These applications of phase conjugation are developed in recent review articles [5].

Various methods of conventional optics have been proposed to build PC mirrors: this is one of the goals of adaptive optical systems. Worth noticing is a recent demonstration of phase conjugator based on an array of corner reflectors [6]. In this article, one considers non-linear optical phase conjugators only.

3 Non-linear optical methods in phase conjugation

Several processes of non-linear optics have been used to perform phase conjugation. One of the first methods was backward Stimulated Brillouin Scattering (SBS) [3] [5] [7]. An intense optical wave interacts with a non-linear medium to create an acoustic wave which propagates collinearly with the incident beam (Fig. 3). Through acoustooptic interactions, the e.m. beam is reflected by the acoustic wave which acts like a moving mirror. Thus an e.m. wave is generated counter-directionally to the input wave. Due to the Doppler effect on the moving mirror, its frequency is down-shifted by a value equal to the acoustic frequency. The analysis shows that the Brillouin gain is maximum for a back-scattered wave conjugate of the incident one. This can be understood if one realizes that the acoustic wavefront is adapted to the incident optical wavefront, i.e. the density variations of the active medium follow the intensity variations of the incident wave. Thus the equivalent mirror follows a geometrical pattern exactly matched to the incident wavefront, and reflects it back on itself (Fig. 3). In some cases, the reflectivity of this "Brillouin mirror" can approach unity [3] [8]. The main advantage of this technique is that it does not require any auxiliary beams. There are related methods like stimulated Raman and Rayleigh scattering. In all these methods, the re-radiated field is amplified from e.m. vacuum fluctuations, and the amplification maximum is obtained for a conjugate field. For this reason, these techniques are limited to very intense optical pulses.

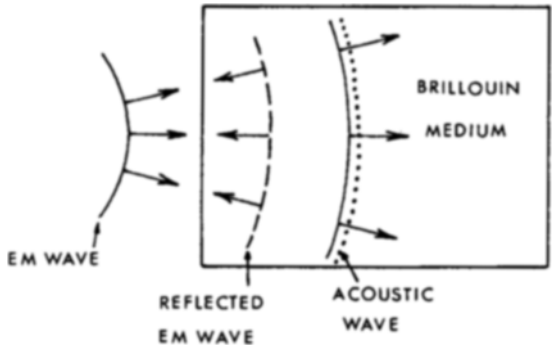


Fig. 3
Backward stimulated Brillouin scattering. The incident e.m. wave generates an acoustic wave in the nonlinear medium, and is reflected by it.

Contrary to the above methods, there is another class of conjugators which rely on the non-linear mixing of several e.m. waves. For instance, in three-wave mixing [9], the active medium interacts with two co-propagating beams at frequencies ω and 2ω. Via absorption of one photon of frequency 2ω, and emission of a photon of frequency ω, a non-linear polarization is driven at frequency ω, which radiates in the *forward* direction an e.m. field, whose phase is opposite to that of the incident (ω) field. Let us notice that this conjugator works in *transmission*, and does not behave like a mirror. This method, which has been demonstrated in lithium formate [10], presents two serious limitations: (i) there are severe restrictions on the angular divergence α of the input beam to be rectified, since the phase matching is satisfied in the forward direction only. If L is the length of the sample cell and λ the optical wavelengh, α must satisfy $\alpha^2 < \lambda/L$ ($\simeq 1^\circ$ for L = 3 mm and $\lambda = 1$ μm). (ii) Three-wave mixing processes can be carried out only in media lacking inversion center, because they need a non-zero second-order susceptibility, $\chi^{(2)}$. There are no such restrictions for degenerate four-wave mixing processes, which are presented in detail in the next sections.

4 Degenerate four-wave mixing

In degenerate four-wave mixing (DFWM), the active medium is irradiated by a standing "pump" wave (frequency ω, wavevectors $\vec{k}_1 = \vec{k}$ and $\vec{k}_2 = -\vec{k}$) and by a probe, or "object" wave, which is to be rectified (frequency ω, wavevector $\vec{k}_0$. See Fig. 4). By absorption of two oppositely propagating pump photons, and emission of a probe photon, the nonlinear medium is able to re-emit a fourth photon of frequency $\omega_r = \omega$ and wavevector $\vec{k}_r = -\vec{k}_0$. In this process, both energy (since every photon carries the same energy, $\hbar\omega$) and linear momentum are conserved (there is absorption of two opposite momentum quanta $\hbar\vec{k}$ and $-\hbar\vec{k}$, and emission of two quanta $+\hbar\vec{k}_0$ and $-\hbar\vec{k}_0$). For this reason, in isotropic media, the phase-matching of this nonlinear process is satisfied independently of the probe beam direction, $\vec{k}_0$.

To see that the re-emitted field is conjugate of the probe field, we have to calculate the nonlinear polarization responsible for the re-radiated field. Let us suppose that the incident e.m. field $\vec{E}$ is the sum of three plane waves ($\mu = 0, 1, 2$. Fig. 4):

$$\vec{E}_\mu = \frac{1}{2}\vec{\epsilon}_\mu \, e^{i\Phi_\mu} + \text{c.c.} \qquad (5)$$

where

$$\Phi_\mu = \omega_\mu t - \vec{k}_\mu \cdot \vec{r} + \varphi_\mu \qquad (6)$$

and

$$\vec{\epsilon}_\mu = \epsilon_\mu \vec{e}_\mu \qquad (7)$$

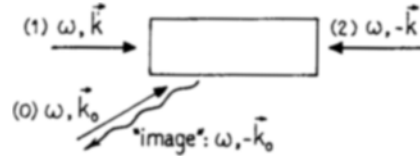


Fig. 4 Configuration of backward degenerate four-wave mixing (DFWM).

ϵ_μ, φ_μ and $\vec{e}_\mu$ are respectively the amplitude, phase and polarization of wave μ. The properties of the re-radiated field are contained in the third-order susceptibility of the medium, $\chi^{(3)}$ [11]. Among the various contributions to the induced non-linear polarization ($\chi^{(3)} \cdot \vec{E} \cdot \vec{E} \cdot \vec{E}$, where $\chi^{(3)}$ is a tensor of fourth rank), let us consider the following one:

$$\vec{P}_r = \frac{1}{8}\chi^{(3)} \cdot \vec{\epsilon}_1 \, e^{i\Phi_1} \cdot \vec{\epsilon}_2 \, e^{i\Phi_2} \cdot (\vec{\epsilon}_0 \, e^{i\Phi_0})^* + \text{c.c.}$$

$$= \vec{p}_r \, e^{i(\omega t + \vec{k}_0 \cdot \vec{r} + \varphi_1 + \varphi_2 - \varphi_0)} + \text{c.c.} \tag{8}$$

with

$$\vec{p}_r = \frac{1}{8}\chi^{(3)} \cdot \vec{\epsilon}_1 \cdot \vec{\epsilon}_2 \cdot \vec{\epsilon}_0^* \tag{9}$$

The corresponding macroscopic dipole polarization is matched to radiate a field at frequency ω, wavevector $-\vec{k}_0$ and having a phase, $\varphi_r = \varphi_1 + \varphi_2 - \varphi_0$, which varies in opposite sense to the probe phase φ_0. The important point is that, independently of the probe wavevector $\vec{k}_0$, a phase-conjugate field is re-emitted in opposite direction to the incident field. Thus the operation of this PC mirror is not limited by phase-matching conditions, and can be used to reflect strongly aberrated waves.

Several characteristics of conjugators based on degenerate four-wave mixing (DFWM) can be emphasized:

(i) As regard wavevector and phase, DFWM conjugators behave like an ideal one (section 2). But there is no particular reason for the polarization of the reflected beam to be the complex conjugate of the incident one, $\vec{e}_0$. The polarization characteristics of the conjugate beam may be deduced from the laws of conservation of the global angular momentum of the e.m. field [12] (See section 9) and are contained in the vectorial properties of $\vec{P}_r$: if propagation effects can be neglected, the amplitude of the reemitted field follows:

$$\vec{\epsilon}_r \sim i\,\vec{p}_r \tag{10}$$

(ii) As shown by the energy conservation considerations presented at the beginning of this section, the incident probe field is *amplified*, simultaneously to the emission of the PC field. If the gain is large enough, the behaviour of the medium becomes critical (unstable) and there is a possibility of *mirrorless oscillation* [13]. This will be discussed in Section 10. This also implies that the reflectivity of the DFWM conjugator may be larger than one, contrary to Brillouin mirrors reflectivity.

(iii) The phase-matching of the DFWM process is exactly satisfied for equal pump and probe frequencies. In the case of a pump-probe frequency detuning, the phase-matching is lost, and the mirror reflectivity decreases with increasing detuning. Thus DFWM conjugators can be considered as narrow-band *optical filters* working in reflexion [14].

The first demonstrations of DFWM phase-conjugation have been performed in dyes [1], Si [2], and CS_2 [15], as the active media. Since then, a wide variety of materials (solids, liquids and gases), has been used for this purpose [5].

The choice of a nonlinear medium presenting a large $\chi^{(3)}$ value for the incident wavelength is favorable to the DFWM efficiency [16]. For instance, $\chi^{(3)}$ enhancements induced by the proximity of a resonance allow one to improve the PC mirror reflectivity: this is the case when an optical resonance alters the absorption (nonlinear absorption – or saturation) or the dispersion of the medium (optical Kerr effect). Photorefractive effects in electro-optic crystals, generation of electron-hole pairs in semiconductors, optically-induced thermal effects in liquids can also be linked to this general class of $\chi^{(3)}$ enhancement via single-photon absorption. As it will be seen, in all these cases the DFWM process may be interpreted in terms of real-time holography (simultaneous writing and reading of holographic gratings). A different class of DFWM processes (without holographic interpretation) originates in resonant or near-resonant two-photon absorption. This second class is closely connected to two-photon spectroscopy (in particular, Doppler-free two-photon spectroscopy [17]).

5 One-photon resonantly enhanced DFWM and real-time holography

The physical processes responsible for one-photon-resonant DFWM can be apprehended by using a simple two-level model. The generalisation to multilevel structures, or transition between energy bands (in solids or molecular liquids) is straightforward. The time-ordering of interactions between the e.m. field and the active medium is imposed by the proximity of a resonant transition for the incident frequency. If one reminds that two pump photons must be absorbed and one probe photon emitted, thus the ordering necessary to make every step quasi-resonant is the following one: a first interaction with either pump field ($\vec{k}$, for instance), a second interaction with the probe $\vec{k}_0$, and the third one with the other pump, $-\vec{k}$ (Fig. 5). The net result is to generate an optical polarization phase-matched in direction $-\vec{k}_0$. Similarly there is an interaction ordering in which the two pump fields are exchanged.

In these emission processes, the dominant intermediate step corresponds to the creation in the medium of a spatial modulation of populations (or index). For instance, let us consider the case when the active medium first interacts with pump $\vec{k}$ and probe $\vec{k}_0$. Due to the interference between both waves, the total e.m. field exhibits intensity maxima and minima alternately distributed along equidistant planes, perpendicular to the vector

$$\vec{K} = \vec{k} - \vec{k}_0 \tag{11}$$

and separated by the spatial period

$$\Lambda = 2\pi/K = \lambda/(2\sin\theta/2) \tag{12}$$

where θ is the angle $(\vec{k}, \vec{k}_0)$ and λ the optical wavelength.

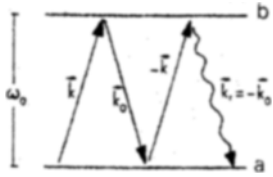


Fig. 5 Physical processes in two-level resonant DFWM (from Ducloy *et al.* [30]).

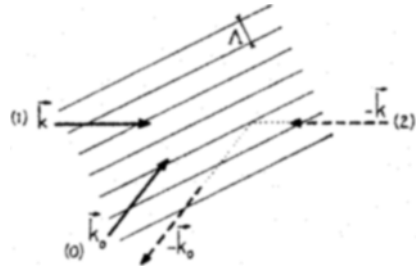


Fig. 6 Creation of a Bragg grating (spatial period Λ) by probe (0) and pump (1), on which pump (2) is diffracted.

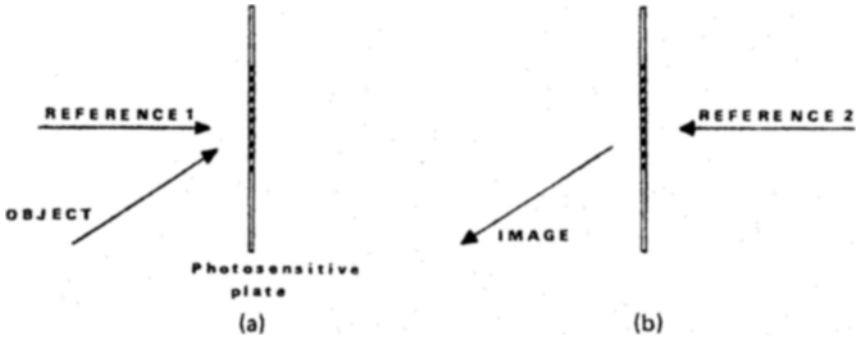


Fig. 7 Two-step holographic analog of DFWM: (a) Hologram recording, (b) Hologram reading.

The effect of this e.m. field distribution is to induce in the interaction volume a spatial modulation of either the populations of the energy levels (in the case of an absorbing medium, on resonance) or the refraction index (for a dispersive medium, in the resonance wings). This modulation pattern can be viewed as a volume grating, of period Λ, impressed in the medium (Fig. 6). The return pump $(-\vec{k})$, incident along a Bragg grating direction, is diffracted in direction $-\vec{k_0}$, to yield the conjugate wave. Let us note that, symmetrically, there is another thick grating produced by probe and pump $(-\vec{k})$ [spatial period, $\lambda/(2\cos\frac{\theta}{2})$], on which pump $\vec{k}$ is diffracted. The analogy with holography has been pointed out by A. Yariv [18]. In a first step ("hologram writing"), reference (1) and object waves (0) produce a thin phase pattern in the photographic plate (Fig. 7a). During the hologram reading, the return reference wave (2) is diffracted by this holographic pattern to restore an image which can be superimposed to the original object (Fig. 7b). In comparison, the

DFWM process may be viewed as *real-time holography*, since a thick holographic grating is simultaneously produced and read in the active medium by the three incident waves. This interpretation shows why phase conjugation allows the real-time processing of e.m. fields.

6 Real-time optical image processing and wavefront rectification

Many demonstrations of real-time processing of optical fields based on DFWM processes have been perfomed with a large variety of materials [5]. Within a few variants, they rely on the experimental set-up sketched in Fig. 8. This is the basic DFWM configuration, in which an image is impressed onto the probe wavefront by transmission through (or reflexion on) an object (testcard, slide, resolution chart, etc...). An aberrating medium (irregular glass plate, transparent scotch-tape, ...) disturbs the object wavefront and, with the help of beam splitters, the conjugate image is observed, either distorted before traveling back through the phase-disturbing medium, or restored after a second transit into this medium (Fig. 8). As an example, Fig. 9 shows optical wavefront rectification performed

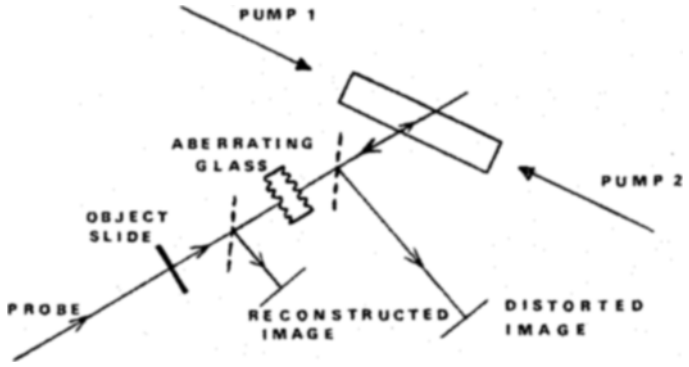


Fig. 8 Principle of the experimental set-up used to demonstrate real-time wavefront rectification.



Fig. 9 Demonstration of DFWM wavefront rectification at 640 nm in a neon discharge: (left) conjugate image, (center) distorted image, (right) reconstructed image [D. Bloch, R.K. Raj and M. Ducloy, unpublished work].

in our laboratory at $\lambda = 640$ nm, with a single-mode c.w. dye laser as the light source and a low-pressure neon discharge as the nonlinear medium. In this figure, the image of a razor grid is shown: (a) directly on the conjugate beam (without disturbing medium); (b) distorted after *one* transit in the aberrating medium; (c) rectified after *two* transits (back and forth) in the medium. The physical process responsible for DFWM at 640 nm is resonant saturated absorption of metastable neon atoms ($1\,s_5 \rightarrow 2\,p_9$) and will be elaborated on in the next section.

A second example of optical image processing is shown in Fig. 10. In this experiment performed by Huignard and collaborators [19], the light source is a c.w. Ar^+ ion laser ($\lambda = 514$ nm) and the active medium is a $Bi_{12}\,Si\,O_{20}$ (BSO) crystal. Figure 10 shows the distorted image, the reconstruction process, and also the drastic effect of a small misalignment (1.5 mrd) of the two pump waves. In the case of BSO, the physical mechanism responsible for PC emission is the photorefractive effect in electro-optic crystals. The light irradiation excites photocarriers (electrons in the case of BSO) from traps in the energy gap to the conduction band. These free photo-carriers, after migrating in the crystal either by diffusion or by drift in an external d.c. field, are retrapped in acceptor centers. Thus a space charge density, proportional to the irradiation energy (below saturation), builds up, locally producing an electric field. Via the linear electro-optic effect, this space charge field causes a refractive-index change: the light irradiation fringe pattern produces an index grating in the crystal interaction volume [20]. The recording time (and erasing time) of this grating is inversely proportional to the incident power, because the efficiency of the writing process increases linearly with the irradiation energy. The time constant is $\sim 1 - 2$ ms for a power density of 1 mW/mm^2, and saturation occurs at about 1 mJ/cm^2.

Fig. 10 Wavefront rectification at 514 nm in a BSO crystal: (a) direct imaging through aberrating glass plate, (b) reconstruction process, (c) effect of a pump misalignment by 1.5 mrad (from Huignard *et al.* [19]).

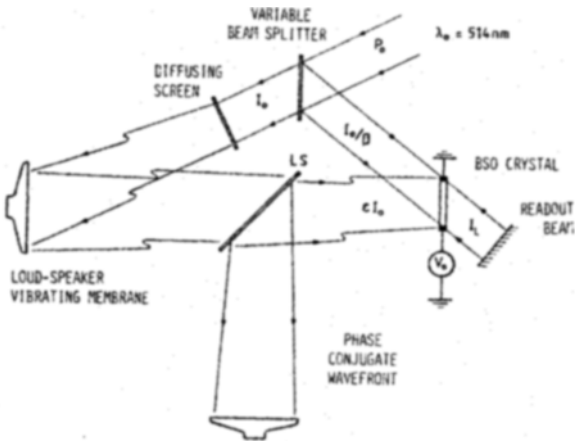


Fig. 11
Optical set-up for dynamic holography and real-time visualization of diffuse vibrating structures (here a loudspeaker membrane – from Marrakchi *et al.* [21]).



Fig. 12 Time-averaged interferogram of a diffuse vibrating object: mode pattern visualization of a loudspeaker membrane excited at different frequencies a) at rest, b) 4 kHz, c) 8 kHz (from Marrakchi *et al.* [21]).

Another application of DFWM conjugation is the real-time recording and reading of holograms of three-dimensional (3-D) diffuse objects. For example, BSO crystals have been used to visualize the mode pattern of diffuse vibrating structures [21]. In this experiment (Fig. 11), the object wave is obtained by reflexion of a diffusing beam on the test object – here a loudspeaker membrane –. At rest, the conjugate image reproduces the 3-D hologram of this membrane (Fig. 12). When this membrane is excited at some driving frequency F, the conjugate image discloses dark fringes which visualize the vibration modes of the membrane. Indeed, the moving parts of the membrane introduce a time-dependence in the phase of the object beam. When these time variations are fast compared with the response time of the BSO index grating, this grating cannot build up sufficiently to diffract the reference

beam [21]. This technique can be used for the non-destructive testing of mechanical structures. Other optical functions can be perfomed like double-exposure interferometry [22], edge enhancement of an optical image [23] (filtering of low spatial frequencies by using a saturating object beam), spatial convolution and correlation [24], etc.

7 Spectroscopic applications of degenerate four-wave mixing

7.1 Grating spectroscopy

Let us assume that, in Fig. 4, probe (0) and pump (1) are two short, time-coincident optical pulses, and that pump (2) is time-delayed. The intensity of the conjugate pulse versus time delay allows one to observe the evolution of the transient holographic grating, and provides a powerful tool to explore relaxation and diffusion processes. This technique is closely related to a large research field known as grating spectroscopy, in which transient diffraction gratings are created and subsequently probed with optical pulses (see *e.g.* the general reviews by Eichler [25], and Vinetskii *et al.* [20]).

The grating decay is mainly affected by two processes. (i) the "Natural" or "intrinsic" decay (radiative decay, recombination time, collisional relaxation) which does not depend on the grating features (decay time, τ). (ii) the grating "washing-out" induced by the motion of the excited centers through the grating fringes (diffusion, thermal motion in gases). It depends on the grating period, Λ, and thus, on the angle θ [Eq. 12]. The characteristic decay time is the time needed for an active center to travel across one grating period. For instance, a diffusion-induced grating decay (generally predominant in solids, liquids or high-pressure gases) is exponential with a time constant.

$$\tau_D = \Lambda^2/(4\pi^2 D) = (K^2 D)^{-1} \tag{13}$$

where D is the ambipolar diffusion constant. On the opposite, for low-pressure gases, the thermal motion produces a non-exponential decay of the form:

$$e^{-(Kut/2)^2} \tag{14}$$

(for a Maxwellian velocity distribution, with mean thermal velocity, u). The characteristic time is now

$$\tau_M = 1/(Ku) \tag{15}$$

In both cases, one sees that natural decay and motional decay can be discriminated by varying Λ, i.e. θ. In this way, transient DFWM has been used to analyze free carriers diffusion in Si [2], exciton diffusion in GaAs [26], thermal diffusivity in liquids and glasses [27], fluorescence lifetime in ruby [28], etc.

In multilevel resonant transition, a sublevel structure in one of the energy levels can induce quantum interference beats in the time-evolution of the transient population

gratings. These beats produce an intensity modulation of the conjugate pulse as a function of the delay time. Such Zeeman quantum beats on the sodium D_1 line have been observed by Yamada *et al.* [29].

In the steady-state regime, the grating motional decay affects the DFWM efficiency, and may be responsible for a sharp angular dependence in the conjugate wave amplitude. For instance, in presence of diffusion, this amplitude is proportional to

$$\left(\frac{1}{\tau}+\frac{1}{\tau_D}\right)^{-1} = \left(\frac{1}{\tau}+K^2D\right)^{-1} \simeq \left(\frac{1}{\tau}+k^2D\,\theta^2\right)^{-1} \tag{16}$$

(for $\theta \ll 1$). In gases, a rapid angular dependence of the DFWM efficiency exists also, but the phenomenon is further complicated by the Doppler effect which affects the emission lineshape [30], [31], as seen in the next section. This θ-dependence, which has been observed in Si by Jain *et al.* [32], and Na vapor by Humphrey *et al.* [33], introduces severe limitations on the angular divergence of distorted beams to be rectified [34].

7.2 Doppler-free conjugate emission in resonant gas media

In gas media, when the frequency of the incident beams is close to an atomic resonance frequency, ω_0, the PC emission lineshape is mainly governed by the Doppler effect. In the case of the two-level system of Fig. 5, one has to write the resonance conditions, in the atomic rest frame, for one photon absorption,

$$\omega - \vec{k}\cdot\vec{v} = \omega_0 \tag{17}$$

and for three-photon transitions to the excited state (see Fig. 5):

$$(\omega-\vec{k}\cdot\vec{v})-(\omega-\vec{k}_0\cdot\vec{v})+(\omega+\vec{k}\cdot\vec{v}) = \omega+\vec{k}_0\cdot\vec{v} = \omega_0 \tag{18}$$

($\vec{v}$ is the atomic velocity). As seen above, the PC emission is maximum for $\theta \ll 1$. In this case, pumps and probe are nearly collinear, and define a common axis ($\vec{k}\approx\vec{k}_0$), along which there is a velocity selection by the three incident beams: Eqs. (17) and (18) are both satisfied for $\vec{k}\cdot\vec{v}=0$ and $\omega=\omega_0$; *i.e.* for $\omega=\omega_0$, atoms with zero axial velocity are simultaneously resonant for the three beams, and the emission intensity is maximum. This velocity selection implies the Doppler-free character of the PC emission. Indeed, a density-matrix calculation [30] shows that the velocity-averaged third-order susceptibility is proportional to

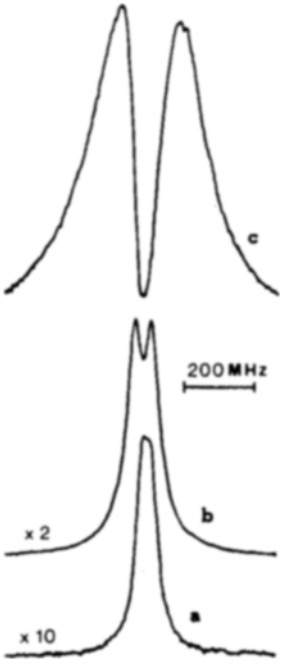
$$\chi^{(3)} \sim \frac{1}{\omega-\omega_0-i\gamma} \tag{19}$$

with γ the transition homogeneous linewidth. When propagation effects are negligible ("optically thin sample") the emission intensity is proportional to $|\chi^{(3)}|^2$ [see Eqs (9) – (10)]. Doppler-free lineshapes have been first observed in Na by Liao *et al.* [35], and subsequently in a number of gas media, including SF_6 [36], excited Ne [37], [38] and Hg [39]. Fig. 13 shows PC emission lineshape observed

in a Ne discharge at $\lambda = 640$ nm (resonant transition between the metastable level $1s_5$ and the radiative level $2p_9$). At low pump power levels (0.1 mW/mm^2), the emission lineshape is a Doppler-free Lorentzian, as predicted by Eq. (19).

Note that this Doppler-free character is also valid for *nearly-degenerate* four-wave mixing (NDFWM: pump and probe frequencies slightly detuned) and demonstrates that PC mirrors based on resonant FWM can be used as ultra-narrow reflexion filters [30] [40] [41]. The filter bandwidth is mainly limited by the atomic relaxation rates (γ) but the acceptance angle is limited to very small values of θ ($\theta \lesssim \gamma/ku$ [30]). When θ increases, the reflectivity decreases like $(\sin \theta)^{-4}$ (see previous section and Ref. [34]) and the filter bandwidth undergoes a Doppler broadening, increasing like $ku \sin \theta$ [30].

With increasing pump powers, the emission lineshape broadens and subsequently splits in two components (Fig. 13, b, c). This double-peak structure, which must be ascribed to the higher-order contributions to the susceptibility ($\chi^{(5)}$; $\chi^{(7)}$ etc. ...), is a typical effect of the inhomogeneous broadening coming from the velocity distribution: for stationary atoms, non-perturbative calculations predict a single peak, independently of the pump intensity [42]. This saturation behavior has been further explored by means of a powerful technique relying on a heterodyne detection of nearly degenerate FWM [43] (Fig. 14). For a probe wave detuned by δ



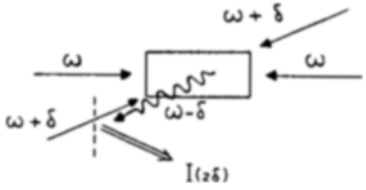


Fig. 14 Basic scheme for heterodyne detection of four-wave mixing (from Bloch *et al.* [37]).

Fig. 13
Conjugate emission lineshape at 640 nm, in a Neon discharge (transition $1s_5 - 2p_9$). Probe intensity $\simeq 10^{-2}$ mW/mm^2; pump intensity: (a) 0.1 mW/mm^2 (b) 0.2 mW/mm^2 (c) 2.5 mW/mm^2 (from Bloch *et al.* [37]).

from the pump frequency, the conjugate wave is reemitted at frequency $2\omega-(\omega+\delta)=\omega-\delta$. The conjugate field may thus be detected through its heterodyne beat (at frequency 2δ) with the return probe wave acting as a local oscillator (Fig. 14). This beat is monitored by a phase-sensitive (lock-in) detector which directly provides signals proportional to the conjugate field *amplitude* (either in phase or in quadrature), and thus to the nonlinear susceptibility χ_{NL} (Fig. 15). At low pump intensities, χ_{NL} follows Eq. (19) and thus obeys to Kramers-Kronig relations. As shown by Fig. 15a, real and imaginary parts have the same amplitude. At higher intensities (Fig. 15b), these relations break down and the dispersion component (Re χ_{NL}) takes over the absorption component, Im χ_{NL}. It implies that the emission lineshape of Fig. 13c should be ascribed to the dispersive character of saturated susceptibilities in resonant four-wave mixing ($|\chi_{NL}|^2$ behaves approximately like the square of a dispersion curve) [44].

7.3 High-Frequency Heterodyne Spectroscopy

High-frequency heterodyne Doppler-free spectroscopy [45] covers the particular field in which *collinear, nearly-degenerate* four-wave mixing is used to perform high-resolution spectroscopy. The basic geometry is shown in Fig. 16. A two-frequency ($\omega \pm \delta/2$) saturating beam and a counterpropagating (ω) beam interact within the sample cell. Through resonant four-wave mixing processes, two conjugate fields at frequencies $\omega+\delta$ and $\omega-\delta$ are re-radiated in the direction of the ω beam [45], and interfere with this beam to yield a heterodyne beat at frequency δ. A straightforward generalisation of Eqs. (8)–(10) shows that the beat amplitude is proportional to

$$i\chi^{(3)}(\omega+\delta)-i\chi^{(3)}(\omega-\delta) \tag{20}$$

Thus, as in the previous section, by using phase-sensitive detection, one can observe either non-linear dispersion contributions,

$$\mathrm{Re}\,[\chi^{(3)}(\omega+\delta)-\chi^{(3)}(\omega-\delta)] \tag{21}$$

or non-linear absorption,

$$\mathrm{Im}\,[\chi^{(3)}(\omega+\delta)+\chi^{(3)}(\omega-\delta)] \tag{22}$$

In general, the optical dipole polarizations at frequencies $\omega+\delta$ and $\omega-\delta$ are not simultaneously resonant, and the beat signal lineshape exhibits Doppler-free frequency doublets, in absorption or in dispersion, according to the detection phase.

For a resonant two-level system (Fig. 5), velocity-selection conditions for one-photon and three-photon processes [similar to Eqs. (17)–(18)] allow one to show that the doublet peaks are centered at [45, 46]

$$\omega=\omega_0\pm 3\delta/4 \tag{23}$$

Such absorption and dispersion doublets are shown on Fig. 17, for an I_2 sample irradiated by an Ar^+ laser (λ = 514 nm) [46–48].

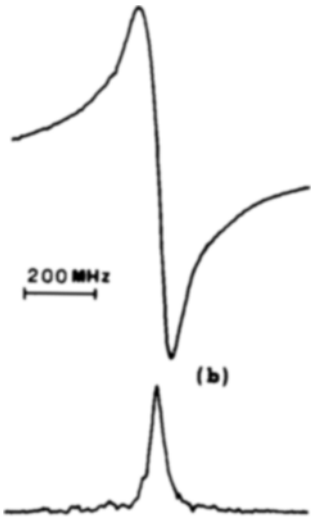


Fig. 15 Heterodyne detection of PC emission at 640 nm in a Ne discharge (phase and quadrature). Frequency detection, $2\delta = 44$ MHz. Pump intensity: (a) 0.1 mW/mm^2 (b) 1 mW/mm^2. The probe intensity is one tenth of the pump intensity (from Bloch *et al.* [37]).



Fig. 16 Basic scheme for high-frequency Doppler-free heterodyne spectroscopy (collinear, nearly-degenerate four-wave mixing) (from Ducloy *et al.* [45]).

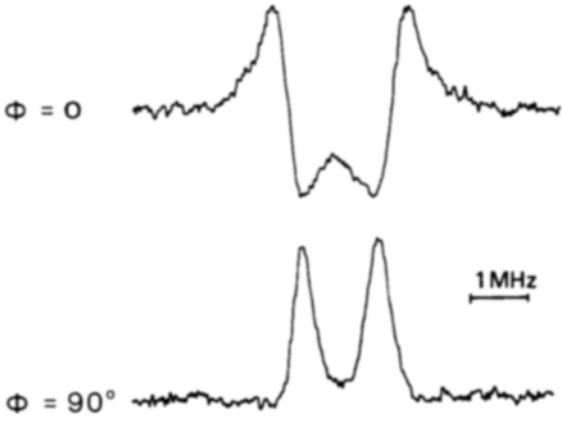


Fig. 17
Resonance lineshape in I_2 heterodyne spectroscopy at $\lambda = 514$ nm. Frequency detection, $\delta = 1$ MHz. Depending on the detection phase, the heterodyne beat signal yields either nonlinear absorption or dispersion doublets (from Raj *et al.* [46]).

For a frequency splitting, $3\delta/2$, smaller than the natural linewidth, the doublet is not resolved, and the dispersion contribution cancels [cf. Eq. (21)]. The nonlinear absorption stays alone, reducing to ordinary "saturated absorption" spectroscopy [49], which thus can be viewed as "heterodyne" detection (at zero frequency, $\delta \to o$) of collinear degenerate four-wave mixing.

Another point of view consists in noting that the two-frequency saturating beam is amplitude-modulated at frequency δ, and thus induces in the populations of the resonant levels a time-modulation, or "pulsation grating". In turn, this population "pulsation grating" modulates the transmission of the counter-propagating wave, thus generating side-bands at frequencies $\omega \pm \delta$. This interpretation underlines the close analogy with the population gratings of non-collinear DFWM (section 5). It also points out the physical origin of the phase delay appearing between the incident amplitude-modulation of the saturating beam, and the induced heterodyne beat, which directly originates in the response time of the atomic populations [45], 46, 50]. This allows us to carry out in the time – (or frequency-) domain, what real-time holography does in the spatial counterpart. In particular, high-frequency optically heterodyned spectroscopy (HFOHS) is a powerful tool for exploring the relaxation dynamics in inhomogeneously – broadened media. Let us quote a few striking applications:

(i) The phase delay of the heterodyne beat signal is induced by the relaxation of the energy levels, and yields a direct measure of their relaxation time (particularly for cross-over resonances in three-level systems [45]). This has been performed in I_2 [46–48] and H [47–50].

(ii) The resonance phase shift also allows one to perform line assignment, particularly when the energy levels have very different lifetimes (for instance, electronic ground state versus excited state in I_2 [48]).

(iii) Cross-relaxation in inhomogeneously-broadened media (like velocity-changing processes in gases) can be analyzed in a detailed way by HFOHS. The Doppler-free character allows one, via an adequate choice of the *optical frequency*, to explore a fixed region of the inhomogeneous line (*e.g.*, a given velocity in gases). Then, the *detection frequency* (δ) and phase delay give access to a particular frequency-domain of the relaxation processes (or evolution processes, more generally). In a way, this method yields the "transfer function" of the nonlinear medium, for every incident optical frequency. It has been used to observe velocity-changing collisions in I_2 [46], in metastable Ne by a closely related technique [51], as well as radiative trapping of the Ne resonance line [52].

Worthnoticing is the shot-noise limited sensitivity which can be reached in HFOHS [50, 53, 54]: the ultimate S/N limit can be reached for detection frequencies δ high enough to make the amplitude noise of the laser source down below the fundamental quantization noise of the signal. This has obvious implications in spectroscopy and metrology [53–55]. HFOHS has also been applied to two-photon spectroscopy [52, 56]. (See next section).

8 Two-photon resonant phase conjugation

An important class of DFWM phase-conjugators originates in resonant or near-resonant two-photon absorption [57–59]. This class has no holographic interpretation (contrary to one-photon resonant DFWM, no volume gratings are induced in the active medium), but relies on the generation of a two-photon coherence. The basic scheme is still that of Fig. 4, but one assumes that the incident frequency is resonant for a two-photon transition ($2\omega \simeq \omega_0$, see Fig. 18). The fact that two pump photons should be absorbed, implies a new interaction ordering. In this ordering the first two field-interactions occur with the standing pump wave, to generate a two-photon coherence which oscillates at frequency 2ω, and is stationary (no spatial dependence). This two-photon coherence is *isotropic, in phase* over all the interaction volume, and *velocity-independent* in gases [30]. The irradiation of this coherence by the object wave $\vec{k}_0$ forces the nonlinear medium to re-radiate in direction $-\vec{k}_0$.

(i) The isotropy property implies that the PC reflectivity does not depend on the angle of incidence of the object beam, θ.

(ii) In gases, the velocity-independence of the two-photon coherence is responsible for the Doppler-free character of the emission lineshape, independently of θ. These two properties should be opposed to the characteristic angular dependence of PC reflectivity and lineshape in one-photon resonant DFWM (Sections 7.1 and 7.2). This is important for wavefront rectification, but is achieved at the expenses of the DFWM reflectivity: most of the experimental observations of two-photon phase conjugation have been carried out with intense optical pulses, for instance in Na [60] and SF_6 [61], hindering any direct evidence of the Doppler-free character of the emission lineshape. In the above works, coherent transients by means of time-delayed optical pulses have been used to measure two-photon relaxation rate ("two-photon free-induction decay") [60–61].

A direct evidence of the Doppler-free emission lineshape has been obtained by using collinear, nearly-degenerate FWM with c.w. irradiation, and heterodyne detection techniques (HFOHS, Section 7.3). The principle is the same as in Fig. 16. The emission peaks at frequencies $\omega \pm \delta$ are now imposed by two-photon absorption conditions:

$$\omega + (\omega \pm \delta/2) = \omega_0$$

$$i.e. \quad \omega = \frac{\omega_0}{2} \mp \delta/4 \qquad (24)$$

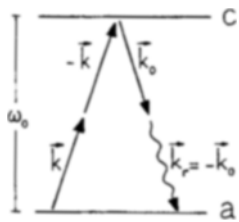


Fig. 18
Physical processes in two-photon resonant DFWM (from Ducloy *et al.* [30]).

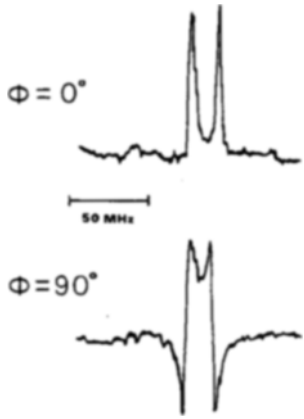


Fig. 19 Resonance lineshape in two-photon heterodyne spectroscopy of Rb at $\lambda = 760$ nm; transition $5S - 7S$; detection frequency, $\delta = 36$ MHz (from Bloch *et al.* [56]).

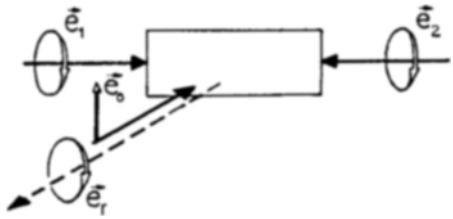


Fig. 20 Polarization properties of a DFWM mirror with circularly polarized pumps: a linearly polarized input field is reflected with a circular polarization.

The emission lineshape exhibits a Doppler-free doublet with splitting $\delta/2$ [45]. Two-photon heterodyne spectroscopy has been demonstrated in excited Neon [52] and in Rubidium [56]. For instance, the $\delta/2$ doublet has been observed on the $5S \rightarrow 7S$ two photon transition of Rb, at $\lambda = 760$ nm (Fig. 19). Two-photon heterodyne spectroscopy could have metrological implications, in particular for the detection of very narrow transitions between ground and metastable states.

9 Polarization properties of phase-conjugate mirrors

As pointed out in Section 4, the polarization vector, $\vec{e}_r$, of the beam reflected from a DFWM conjugator is in general *not the complex conjugate* of the incident polarization, $\vec{e}_0$. The polarization of the PC field should be deduced from the general laws of conservation of the angular momentum. In many cases where the active medium is *isotropic* (gas, liquids, etc. ...), the global angular momentum of the electromagnetic field *alone* must be conserved in the DFWM process, and imposes stringent polarization selection rules [12, 62]. This is particularly obvious when the polarizations of the incident beams are chosen among the principal polarizations (π, σ^+, σ^-) in a fixed quantization frame.

As an example, let us consider the case when the two pump waves are σ^+ circularly-polarized (Fig. 20) [12]. In the DFWM process, two pump photons – each one carrying one angular momentum unit, $\hbar$, along the quantization axis, $\vec{k}$ – are absorbed. These two units can be restituted to the e.m. field only if both probe and conjugate waves are σ^+ polarized: a σ^- polarized input field is not reflected, but a

linearly polarized field (with polarization $\sigma = \frac{\sigma^+ + \sigma^-}{\sqrt{2}}$) is reflected with a circular σ^+ polarization. These selection rules have been verified in Neon [63].

For arbitrary incident polarizations, the polarization of the conjugate beam depends on a number of factors like: nonlinear physical process (one-photon/two-photon resonance), incidence angle, angular momenta of the resonant energy levels, relaxation processes. However, often simple ways exist to characterize the polarization properties of PC mirrors by means of linear or circular dichroism, birefringence, etc. ... [38]. A simple and illustrative example is the one in which the two pumps have the same linear polarization (π), taken as the quantization axis: $\vec{e} = \vec{e}_1 = \vec{e}_2$ (Fig. 21 a). Since a π polarized field carries zero angular momentum along the $\vec{e}$ axis, the conservation of angular momentum obliges a π polarized probe to be reflected with the same polarization. Also a σ polarized probe (*i.e.* having a linear polarization perpendicular to $\vec{e}$, thus carrying + ħ and − ħ units) cannot produce a π polarized conjugate field, and therefore is necessarily reflected with the same σ polarization. In this way, we have defined the *normal axes* of the PC mirror (polarizations unchanged by reflexion). As a rule, the reflexion coefficient is different for these two polarizations ("linear dichroism"), which implies that an incident wave of arbitrary polarization $\vec{e}_0$ is, in general, reflected with a different polarization, $\vec{e}_r$ (Fig. 21 b). By projecting $\vec{e}_0$ along the normal axes, one gets that $\vec{e}_r$ satisfies to:

$$\mathrm{tg}\alpha_r = C\,\mathrm{tg}\alpha_0 \tag{25}$$

where α_i is the angle $(\vec{e}_i, \vec{e})$, and C is the ratio of the (amplitude) reflectivities for the two principal polarizations [38]. Fig. 22 shows the verification of such a relationship on various Neon transitions: one finds $C \simeq 0$ for the $1s_4\ (J=1) - 2p_3\ (J=0)$ transition ($\lambda = 607$ nm) and $C \simeq 0.23$ for the $1s_5\ (J=2) - 2p_6\ (J=2)$ transition ($\lambda = 614$ nm).

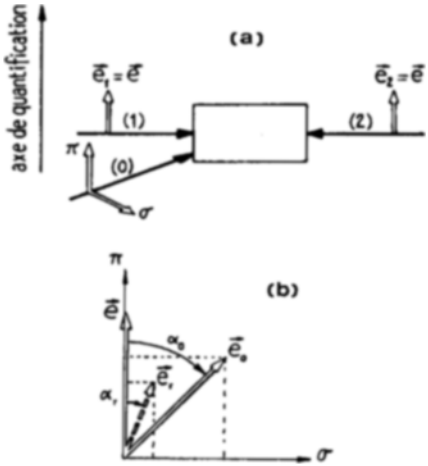


Fig. 21
Polarization properties of a PC mirror with linearly polarized pumps (a) General scheme (b) Geometry of the polarizations of the incident and reflected waves.

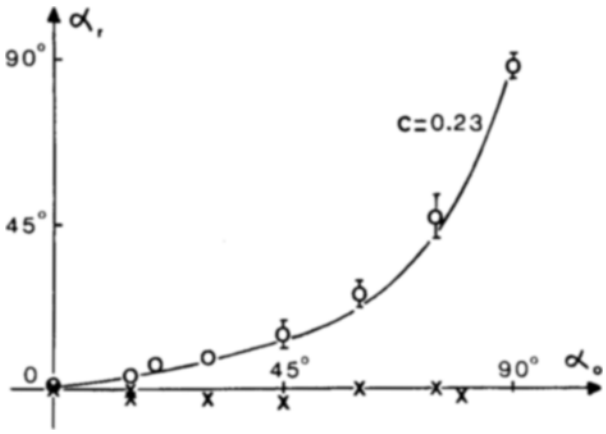


Fig. 22 Polarization rotation of the reflected signal for parallel pump polarizations (X) $\lambda = 607$ nm, neon transition $1s_4 - 2p_3$; (0) $\lambda = 614$ nm, $1s_5 - 2p_6$. The solid curve follows $tg\alpha_r = 0.23\ tg\alpha_0$ (from Ducloy *et al.* [38]).

To evaluate C, one has to go into the details of both the nonlinear processes and the grating relaxation. An important difference between π and σ probe polarizations is that, in the first case, the grating created in the interaction volume is a *population grating* (since all the beams have the same polarization), while in the second case, owing to the orthogonal polarizations, the grating is a pure *coherence grating, i.e.* the atomic system is excited in a linear superposition of Zeeman sublevels exhibiting a spatial modulation [38] [63–65]. What simplifies considerably the analysis of these phenomena is that the grating motional decay [Section 7.1, Eqs. (13–15)] generally overcomes radiative or collisional decays, thus imposing a single relaxation time, τ_M, to all the physical observables (populations, coherences...). One shows that in this case, C depends only on the J values and describes adequately the experimental results [38] [66]. Coherence gratings have also been observed on the Na D-lines [64, 65]. In a similar manner, diffusion-induced motional decay in solids has been analyzed by DFWM polarization studies [67].

Finally, let us note a way of getting *complete* phase-conjugation, i.e. producing $\vec{e}_r = \vec{e}_0^*$. This is possible in a number of cases in which both pumps are circularly polarized but mutually orthogonal (σ^+, σ^-). In that case, the net angular momentum of two absorbed pump photons is zero, which implies that a σ^+ polarized probe is reflected with σ^- polarization, and vice-versa. Also a π polarized beam is reflected with the same polarization. Such a full spatial-phase reversal has been obtained in CS_2 by Martin *et al* [68]. To get this full phase conjugation for an arbitrary input polarization needs that the DFWM reflectivity is independent of the polarization vector (π, σ^+, σ^-). This is in particular obtained in resonant gas media, when the motional decay time, τ_M, governs the grating relaxation [63].

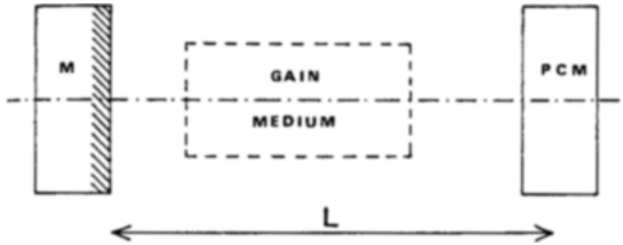


Fig. 23 Principle of a phase-conjugate resonator (M: ordinary mirror; PCM: phaseconjugate mirror).

10 Phase-conjugate resonators

Phase conjugate resonators (PCR) are optical resonators in which one (or several) of the cavity mirrors are replaced by phase-conjugate mirrors. Fig. 23 shows the simplest example of this kind of resonator, a Fabry-Perot cavity with a PC mirror (PCM) at one end, an ordinary mirror (M) at the other end, and possibly an intracavity gain medium. Such PCR have been studied both theoretically [69–72] and experimentally [70, 73]. Their properties depend partly on the operation of the PCM. Let us suppose first that there is no frequency shift produced in the reflexion over the PCM (for instance, with a DFWM conjugator operating at the pump frequency). In that case,

(i) the PCR is *unconditionally stable*. Due to the replication of the incident wavefront by the PCM, the resonator is aligned independently of the curvature radius of the ordinary mirror (M), and of any disturbing elements introduced inside the cavity. However the mode transverse structure will depend on the PCM size and intracavity elements [71]. Such resonators should be able to optimize the energy extraction from an intracavity amplifying medium.

(ii) As regard longitudinal modes, there is no frequency condition involving the cavity length, L. Indeed, the phase shift kL.accumulated in one propagation direction is reversed by the PCM, and thus canceled during the return way. The cavity tuning is obtained independently of the length, in contrast to ordinary resonators.

However, this is no longer true when the operating frequency is detuned (by δ) from the PCM center frequency. In that case, an $\omega+\delta$ wave incident on the PCM is reflected with frequency $\omega-\delta$, and vice-versa (Section 7.2). Therefore, stable PCR operation is possible only for a two-frequency field:

$$E = \epsilon_{\pm}\, e^{i[(\omega\pm\delta)t-\vec{k}\cdot\vec{r}\,]} \tag{26}$$

By writing that the e.m. field is globally unchanged after one cavity round trip, one gets relations of the form:

$$\epsilon_+ = \epsilon_-^* \, e^{-i\delta \frac{2L}{c}}$$

$$\epsilon_- = \epsilon_+^* \, e^{i\delta \frac{2L}{c}} \tag{27}$$

producing the condition

$$e^{i\delta \frac{4L}{c}} = 1, \; i.e. \; \delta = n2\pi \frac{c}{4L} \tag{28}$$

Such a frequency condition invoking four cavity lengths is easily interpreted by realizing that, due to the frequency-flipping nature of the PCM, it needs two cavity round trips for one field component to get back its original frequency and phase. Such frequency sidebands governed by Eq. (28) have been predicted by Belanger *et al* [72], and beautifully observed by Lind and Steel [73] in the c.w. operation of a PCR, using a DFWM conjugator at the Na D_2 line as the PC mirror, and an Ar^+ laser-pumped dye as the gain medium. However, note that this sideband generation is limited to the first harmonics, by the narrow-band frequency-filtering character of DFWM mirrors [Sections 4 and 7.2] [14].

The possibility of PCR oscillation *without intracavity gain medium* has been noted by Yariv and Pepper [13]. This is connected to the fact that in DFWM mirrors (i) simultaneously to the emission of a conjugate wave, the input field is amplified (ii) the PCM reflectivity may exceed unity (mirror gain, cf. Section 4). For very large gains, the PCM acts both like a mirror and a gain medium, and may induce a spontaneous oscillation linked to the ordinary mirror. This has been observed in several experiments using intense optical pulses, and in a Ba TiO_3 crystal with a low-power c.w. argon laser by Feinberg and Hellwarth [74]. In that case, the c.w. mirror gain can be larger than 100! Ba TiO_3 has also been used to observe different types of spontaneous oscillation (like unidirectional ring oscillator, etc...) [75], using two-wave mixing processes [20].

11 Conclusion

In this article, we have reviewed the basic physics, and some of the applications of nonlinear optical phase conjugation. The applications considered here span real-time adaptive optics and imaging (image and information transmission in aberrating media, wavefront rectification, image amplification, automatic pointing and focusing on targets, real-time holography, ...), optical spectroscopy (transient and c.w. grating spectroscopy, multiphoton transitions, high-sensitivity Doppler-free spectroscopy ...), new classes of "mirrors" (frequency-and polarization-selective) and of resonators ("open" resonators with spontaneous oscillation, PC resonators).

This review has left aside a number of important topics like collision-induced DFWM, forward DFWM, DFWM by photon echoes, phase-conjugation in optical fibers and waveguides, conjugate interferometry, photon statistics of the PC field, etc... (See e.g. [5] [76]). A still open field covers the new physical phenomena appearing in the interaction of active media with very intense pump waves: strong saturation regime of the nonlinear response (high-order susceptibilities, nonlinear absorption and dispersion [37]), nonlinear propagation effects (laser-induced instabilities and critical behavior [77], optical bistability and hysteresis in phase-conjugation [78–79]), nonlinear transient response under strong standing waves... Also it has not yet been taken full advantage of the peculiar polarization properties of PC mirrors in PC resonators.

Acknowledgments

The author wishes to thank D. Bloch and R.K. Raj for their contribution to this work. He is grateful to J. Baudon and J.-P. Huignard for stimulating discussions and help in the preparation of this manuscript. This work was supported in part by "Direction des Recherches, Etudes et Techniques" (Paris). The "Laboratoire de Physique des Lasers" is a laboratory associated with the "Centre National de la Recherche Scientifique" (C.N.R.S.).

References

[1] *B.I. Stepanov, E. V. Ivakin* and *A. S. Rubanov*; Sov. Phys. Dokl. 16, 46 (1971).

[2] *J.P. Woerdman*, Opt. Comm. 2, 212 (1970).

[3] *B. Ya. Zel'Dovich, V.I. Popovichev, V. V. Ragul'skii* and *F. S. Faizullov*, JETP Letters,15, 109 (1972); 16, 435 (1972).

[4] *R. W. Hellwarth*, J. Opt. Soc. Amer. 67, 1 (1977).

[5] For reviews on various aspects of phase-conjugation, see: A. Yariv, I.E.E.E. Quant. Electron. QE 14, 650 (1978); B. Ya. Zel'Dovich, N.F. Pilipetskii and V.V. Skunov, Sov. J. Quant. Electron. 8, 1021 (1978); C.R. Giuliano, Physics Today (April 1981); D.M. Pepper, *Laser Focus* (January 1982)

[6] *H.H. Barett* and *S.F. Jacobs*, Opt. Letters 4, 190 (1979).

[7] *V. Wang* and *C.R. Giuliano*, Opt. Lett. 2, 158 (1978).

[8] *M. Slatkine, I.J. Bigio, B.J. Feldman* and *R.A. Fischer*, Opt. Lett. 7, 108 (1982). M.C. Gower and R.G. Garo, Opt. Lett. 7, 162 (1982).

[9] *A. Yariv*, J. Opt. Soc. Am. 66, 301 (1976); Appl. Phys. Lett. 28, 88 (1976).

[10] *P. Avizonis et al.*, Appl. Phys. Lett. 31, 435 (1977).

[11] *N. Bloembergen, Nonlinear Optics* (Benjamin, New York, 1965).

[12] *D. Bloch* and *M. Ducloy*, J. Phys. B.: At. Mol. Phys. 14, L 471 (1981).

[13] *A. Yariv* and *D.M. Pepper*, Opt. Lett. 1, 16 (1977).

[14] *D.M. Pepper* and *R.L. Abrams*, Opt. Lett. 3, 212 (1978).

[15] *S.L. Jensen* and *R. W. Hellwarth*, Appl. Phys. Lett. 32, 166 (1978); D.M. Bloom and G.C. Bjorklund, *ibid*, 31, 592 (1977).

[16] Exhaustive lists of materials and laser wavelengths used in DFWM are given in Ref. [5].

[17] See, *e.g., N. Bloembergen* and *M.D. Levenson* in *High Resolution Laser Spectroscopy*, p. 315 (Springer Verlag, Berlin, 1976).

[18] *A. Yariv*, Opt. Commun. **25**, 23 (1978).

[19] *J. Huignard, J.P. Herriau, P. Aubourg* and *E. Spitz*, Opt. Lett. **4**, 21 (1979).

[20] Note that, in general, the crystal response is non-local, i.e. there is a spatial phase-mismatch between the incident light fringes and the induced index grating. This mismatch is particularly important in *two-wave mixing* experiments, and may produce an energy transfer between the two writing beams.
See e.g. D.L. Staebler and J.J. Amodei, J. Appl. Phys. **43**, 1042 (1972); V.L. Vinetskii, N.V. Kukhtarev, S.G. Odulov, and M.S. Soskin, Sov. Phys. Usp. **22**, 742 (1979); also, Ferroelectrics **22**, 961 (1979).

[21] *A. Marrakchi, J.P. Huignard* and *J.P. Herriau*, Opt. Commun. **34**, 15 (1980).

[22] *J.P. Huignard* and *J.P. Herriau*, Appl. Opt. **16**, 1807, 2796 (1977).

[23] *J.P. Huignard* and *J.P. Herriau*, Appl. Opt. **17**, 2671 (1978); J. Feinberg, Opt. Lett. **5**, 330 (1980).

[24] *J. White* and *A. Yariv*, Appl. Phys. Lett. **37**, 5 (1980).

[25] *H.J. Eichler*: in Festkörperprobleme (Advances in Solid State Physics), Vol XVIII p. 241 J. Treusch (ed), Vieweg Braunschweig 1979

[26] *J. Hegarty, D.M. Sturge, A.C. Gossard* and *W. Wiegmann*, Appl. Phys. Lett. **40**, 132 (1982).

[27] *G. Martin* and *R.W. Hellwarth*, Appl. Phys. Lett. **34**, 371 (1979).

[28] *P.F. Liao* and *D.M. Bloom*, Opt. Lett. **3**, 4 (1978); also H.I. Mandelberg, Opt. Lett. **5**, 258 (1980).

[29] *K. Yamada, Y. Fukuda* and *T. Hashi*, J. Phys. Soc. Jap. **50**, 592 (1981).

[30] *M. Ducloy* and *D. Bloch*, J. Phys. (Paris) **42**, 711 (1981).

[31] *S.M. Wandzura*, Opt. Lett. **4**, 208 (1979).

[32] *R.K. Jain, M.B. Klein* and *R.C. Lind*, Opt. Lett. **4** 328 (1979).

[33] *L.M. Humphrey, J.P. Gordon* and *P.F. Liao*, Opt. Lett. **5**, 56 (1980).

[34] For instance in resonant gases, the DFWM reflectivity may vary by seven orders of magnitude between $\theta = 0$ and $\theta = \pi/2$ (See Ref. [30], p. 715).

[35] *P.F. Liao, D.M. Bloom* and *N.P. Economou*, Appl. Phys. Lett. **32**, 813 (1978).

[36] *D.G. Steel* and *J.F. Lam*, Opt. Comm. **40**, 77 (1981); P. Aubourg et al., Opt. Lett. **6**, 383 (1981).

[37] *D. Bloch, R.K. Laj, K.S. Leng* and *M. Ducloy*, Submitted to Phys. Rev. Lett.

[38] *M. Ducloy, R.K. Raj* and *D. Bloch*, Opt. Lett. **7**, 60 (1982).

[39] *M. Kroll*, Opt. Lett. **7**, 151 (1982).

[40] *T. Fu* and *M. Sargent* III, Opt. Lett. **4**, 366 (1979).

[41] *J. Nilsen* and *A. Yariv*, Appl. Opt. **18**, 143 (1979); J. Opt. Soc. Am. **71**, 180 (1981); Opt. Lett. **6**, 380 (1981).

[42] *R.L. Abrams* and *R.C. Lind*, Opt. Lett. **2**, 94 (1978); **3**, 235 (1978).

[43] *D. Bloch, R.K. Raj, J.J. Snyder* and *M. Ducloy*, J. Phys. Lett. (Paris) **42**, L 31 (1981).

[44] This behavior of χ_{NL} has been inferred by J.P. Woerdman and M.F.H. Schuurmans [Opt. Lett. **6**, 239 (1981)] from a simplified model based on the nonlinear response of *stationary* two-level atoms to a single plane wave. On the opposite an exact density-

matrix calculation (D. Bloch and M. Ducloy, to be published) shows both the eminent role played by the velocity distribution in the behavior of the nonlinear susceptibility, and the quite distinct effects of the saturation induced by either pump wave (directional anisotropy). (See Ref. [37].)

[45] *M. Ducloy* and *D. Bloch*, J. Phys. (Paris) **43**, 57 (1982).

[46] *R.K. Raj, D. Bloch, J.J. Snyder, G. Camy* and *M. Ducloy*, Phys. Rev. Lett. **44**, 1251 (1980).

[47] *D. Bloch*, These de Troisieme Cycle (Universite Paris-Nord, 1980).

[48] *R.K. Raj*, These d'Universite (Universite Paris-Nord, 1980).

[49] See, *e.g., V.S. Letokhov* and *V.P. Chebotayev, Nonlinear Laser Spectroscopy*, Springer Series in Optical Sciences, Vol. 4 (Springer Verlag, Berlin, 1977).

[50] *D. Bloch, R.K. Raj* and *M. Ducloy*, Opt. Comm. **37**, 183 (1981).

[51] *C. Aminoff* and *M. Pinard*, J. Phys. (Paris) **43**, 263 (1982).

[52] *D. Bloch, R.K. Raj, E. Giacobino* and *M. Ducloy*, communication to the First European Conference on Atomic Physics, Abstract V 3 (Heidelberg, April 1981).

[53] *J. Snyder, R.K. Raj, D. Bloch* and *M. Ducloy*, Opt. Lett. **5**, 163 (1980).

[54] *J.L. Hall, L. Hollberg, T. Baer* and *H.G. Robinson*, Appl. Phys. Lett. **39**, 680 (1981); G.C. Bjorklund, Opt. Lett. **5**, 15 (1980).

[55] *G. Camy, C.J. Bordé* and *M. Ducloy*, Opt. Commun. **41**, 325 (1982).

[56] *D. Bloch, M. Ducloy* and *E. Giacobino*, J. Phys. B: At. Mol. Phys. **14**, L 819 (1981).

[57] *M. Matsuoka*, Opt. Commun. **15**, 84 (1975).

[58] *D.C. Haueisen*, Opt. Commun. **28**, 183 (1978).

[59] *T. Fu* and *M. Sargent*, Opt. Lett. **5**, 433 (1980); also G. Agrawal, Opt. Commun. **39**, 272 (1981).

[60] *P.F. Liao, N.P. Economou* and *R.R. Freeman*, Phys. Rev. Lett. **39**, 1473 (1977).

[61] *D.G. Steel* and *J.F. Lam*, Phys. Rev. Lett. **43**, 1588 (1979).

[62] In anisotropic solids, polarization selection rules depend on the peculiar symmetry order of the solid. In the nonlinear process, the solid may globally acquire a non-zero angular momentum, i.e. a torque is exerted on it. See e.g. N. Bloembergen, J. Opt. Soc. Am. **70**, 1429 (1980) and references therein.

[63] *R.K. Raj, D. Bloch* and *M. Ducloy*, to be published.

[64] *J.F. Lam, D.G. Steel, R.A. McFarlane* and *R.C. Lind*, Appl. Phys. Lett. 38 977 (1981).

[65] *S.N. Jabr, L.K. Lam* and *R.W. Hellwarth*, Phys. Rev. A **24**, 3264 (1981).

[66] One predicts that for $J \rightarrow J$ transitions, $C = (J-1)(J+2)/(3J^2+3J-1)$ and for $J \rightarrow J+1$ transitions, $C = -J(2J+4)/(4J^2+8J+5)$. (Refs. [38], [63].)

[67] *D.S. Hamilton, D. Heiman, J. Feinberg* and *R.W. Hellwarth*, Opt. Lett. **4**, 124 (1979).

[68] *G. Martin, L.K. Lam* and *R.W. Hellwarth*, Opt. Lett. **5**, 185 (1980); see also B. Ya Zel'dovich and V.V. Shkunov, Sov. J. Quantum Electron. **9**, 379 (1979).

[69] *I.M. Bel'Dyugin, M.G. Galushkin* and *E.M. Zemskov*, Sov. J. Quantum Electron. **9**, 20, 1198 (1979).

[70] *J. Auyeung, D. Fekete, D.M. Pepper* and *A. Yariv*, IEEE J. Quantum Electron. **QE-15**, 1180 (1979).

[71] *J.F. Lam* and *W.P. Brown*, Opt. Lett. **5**, 61 (1980).

[72] *P.A. Belanger, A. Hardy* and *A.E. Siegman*, Appl. Opt. **19**, 602 (1980).

[73] *R.C. Lind* and *D.G. Steel*, Opt. Lett. **6**, 554 (1981).

[74] *J. Feinberg* and *R. W. Hellwarth*, Opt. Lett. **5**, 319 (1980).

[75] *J. O. White, M. Cronin-Golomb, B. Fischer* and *A. Yariv*, Appl. Phys. Lett. **40**, 450 (1982).

[76] *Nonlinear optical phase conjugation*, edited by R. A. Fischer (Academic Press, 1982, to be published).

[77] *C. Flytzanis* and *C. L. Tang*, Phys. Rev. Lett. **45**, 441 (1980); G. P. Agrawal and C. Flytzanis, IEEE J. Quantum Electron. QE-17, 374 (1981).

[78] *H. G. Winful* and *J. H. Marburger*, Appl. Phys. Lett. **36**, 613 (1980).

[79] *A. Borshch, M. Brodin, V. Volkov* and *N. Kukhtarev*, Opt. Commun. **35**, 287 (1980); **41**, 213 (1982).